Multi-Agent System based Event-Triggered Hybrid Controls for High-Security Hybrid Energy Generation Systems

Dou, Chun-Xia; Yue, Dong; Guerrero, Josep M.

Published in:
I E E E Transactions on Industrial Informatics

DOI (link to publication from Publisher):
10.1109/TII.2016.2618754

Publication date:
2017

Document Version
Early version, also known as pre-print

Multi-Agent System based Event-Triggered Hybrid Controls for High-Security Hybrid Energy Generation Systems

Chunxia Dou, Dong Yue, *Senior, IEEE,* and Josep M. Guerrero, *Fellow, IEEE*

***Abstract*—This paper proposes multi-agent system based event-triggered hybrid controls for guaranteeing energy supply of a hybrid energy generation system with high security. First, a multi-agent system is constituted by an upper-level central coordinated control agent combined with several lower-level unit agents. Each lower-level unit agent is responsible for dealing with internal switching control and distributed dynamic regulation for its unit system. The upper-level agent implements coordinated switching control to guarantee the power supply of overall system with high security. The internal switching control, distributed dynamic regulation and coordinated switching control are designed fully dependent on the hybrid behaviors of all distributed energy resources and the logical relationships between them, and interact with each other by means of the multi-agent system to form hierarchical hybrid controls. Finally, the validity of the proposed hybrid controls is demonstrated by means of simulation results in different scenarios.**

***Index terms*—Hybrid energy generation system, multi-agent system, hybrid control, distributed energy resource, switching control, dynamic control**

NOMENCLATURE

CCCA	Central coordinated control agent
CSC	Coordinated switching control
CVF	Constraint violation function
DERs	Distributed energy resources
DHPN	Differential hybrid Petri-net
FC/MT	Fuel cell and microturbine
HEGS	Hybrid energy generation system
ISC	Internal switching control
MAS	Multi-agent system
MPPT	Maximum power point tracking
PV	Photovoltaic
SAIs	Security assessment indexes
SOC	State of charge
UC	Ultracapacitor
WT	Wind turbine

This work is supported by the National Natural Science Foundation of China under Grant 61573300, 61533010, and Hebei Provincial Natural Science Foundation of China under Grant E2016203374.

C. Dou is with Institute of Advanced Technology, Nanjing University of Posts and Telecommunications, Nanjing, 210023, China, and with Institute of Electrical Engineering, Yanshan University, Qinhuangdao, 066004, China (e-mail: cxdou@ysu.edu.cn)

D. Yue (corresponding author) is with Institute of Advanced Technology, Nanjing University of Posts and Telecommunications, Nanjing, 210023, China (e-mail: medongy@vip.163.com)

J. M. Guerrero is with Department of Energy Technology, Aalborg University, 9220 Aalborg East, Denmark (e-mail:joz@et.aau.dk)

I. INTRODUCTION

THE use of renewable energy resources is an effective solution to energy shortage and environment pollution problems [1], [2]. However, single renewable energy resource usually cannot continuously meet load demand, since its operation status highly depends on natural condition, such as wind speed and solar radiation, and thus resulting in an intermittent power output. In order to make full use of the renewable energy resources to meet load demand with high security, hybrid energy generation systems (HEGSs) are increasingly paid attention. A HEGS is desired to connect various kinds of small distributed energy resources (DERs) into an electrical network to guarantee energy supply with high security. It is able to run in both grid-connected and grid-disconnected modes. In the grid-connected mode, with the support of distribution electrical grid, the HEGS is relatively easy to meet the load demand with high reliability. However, in the grid-disconnected mode, to realize the objective above, effective control mechanism needs to be introduced with taking full consideration of the characteristics of HEGSs [3], [4].

The HEGSs appear typical characteristics of complex hybrid systems mainly because of the following reasons: (i)The frequent start-stop of renewable energy resources results in that these resources present hybrid characteristics including both dynamic and multi-mode switching behaviors [5]-[7]; (ii) To maintain the balance between supply and demand, the storage devices need also to frequently switch their operation modes, and accordingly presenting hybrid characteristics [8], [9]; (iii) The switching between multiple control modes of controllable DERs results in the change of their dynamic behavior, also displaying interactive hybrid characteristics. From the whole system point of view, the HEGSs are multi-source interconnected systems with hybrid characteristics, and thus their control present great challenge.

With respect to control problem of such a complex HEGS, multi-agent system (MAS) technique is certainly one of the most effective means. In the past several decades, a lot of MAS based control approaches regarding HEGSs had been

investigated. However, most of them were focused on dynamic regulation without paying enough attention to the treatment of switching behavior of HEGS [12]-[15]. On the other hand, a few works only focused on MAS based switching control [13]-[15]. In [13], MAS based energy management issue was studied by means of switching control for four operation modes of HEGS. In [14] and [15], the MAS based switching control for storage devices was presented by using logic judgments and fuzzy-logic-rules. As mentioned above, all the relevant research only focused on one aspect of dynamic regulation and switching control without taking full consideration of the both interactive hybrid characteristics.

In addition, with respect to a microgrid, there is a previous research of authors that presented MAS based event-triggered hybrid control [16]. However, when designing switching control strategies, the trigger duration time, switching sequence and time interval had not been fully considered. With respect to a smart grids or a wide-area power system, the references [17], [18] presented MAS based event-triggered control schemes. In [17], the study focused on economic dispatch of smart grids based on distributed event-triggered communication network. In [18,] an event-triggering load frequency control was proposed for multi-area power systems with communication delays. In comparison with this paper, the two references above designed the event-triggered controls from a different point of view to solve entirely different problems.

In this paper, taking full consideration of the hybrid characteristics of HEGS, we propose MAS based hybrid controls for an grid-disconnected HEGS with the following features: (i) switching control, which can switch operation modes of all DERs in a coordinated way to guarantee power supply with high security; (ii) dynamic regulation, which can continuously regulate each DER unit system in a distributed way to guarantee power supply with well dynamic quality; (iii) real-time interactions between discretely switching control and continuously dynamic regulation by means of MAS.

The main contributions are summarized as follows.

(1) A MAS is built to implement hierarchical hybrid controls. Each DER and load unit is associated with a lower-level unit agent to deal with internal switching control (ISC) and distributed dynamic control for the unit system. In the upper level, there is only one central coordinated control agent (CCCA), which is responsible for implementing coordinated switching control (CSC) to ensure high-security energy supply of overall HEGS.

(2) To fully describe the hybrid behaviors of all DERs and the logical relationships between them, a differential hybrid Petri-net (DHPN) model is built. Based on the DHPN model, the following event-triggered hybrid controls are innovatively designed: (i) ISC, where constraint violation functions (CVFs) are proposed as event-triggered conditions; (ii) CSC, where security assessment indexes (SAIs) are designed as event-triggered conditions; (iii) distributed dynamic control strategies corresponding to different control modes. The above hybrid controls can interact real-timely each other by means of the MAS.

In comparison with previous researches, the advantages of the MAS based hybrid controls are as follows.

(1) The two levels of MAS can make use of real-time information interactions to intelligently carry out hierarchical hybrid controls in a distributed coordinated way, and thus the better control performance is easy to be achieved.

(2) The interaction topology of MAS is easy to be dynamically reconstructed when faced with "plug and play" of any DER unit. In this sense, the proposed control scheme is very flexible and scalable.

(3) The event-triggered hybrid controls are designed fully dependent on the hybrid behaviors of all DERs, and accordingly are applied to all DER units. In this sense, the hybrid controls have strong regulating ability when faced with large load disturbances.

(4) In comparison with the previous research of authors [18], in this paper proposed hybrid controls fully consider the trigger duration time, switching sequence and time interval, and thus can switch the operation modes of all DERs in a more reasonable way.

Finally, the validity of the proposed hybrid controls is verified by means of simulation results in different scenarios in comparison with existing state-of-the-art solutions.

II. The MAS Based Control Scheme of HEGS

A HEGS example is shown in Fig. 1, which is divided into two regions: (i) the region 1 that contains a photovoltaic (PV) unit, a battery unit, and a fuel cell (FC) unit combined with a microturbine (MT) unit; (ii) the region 2 that contains a wind turbine (WT) unit, a ultracapacitor (WT/UC) unit, and a group of critical and noncritical loads.

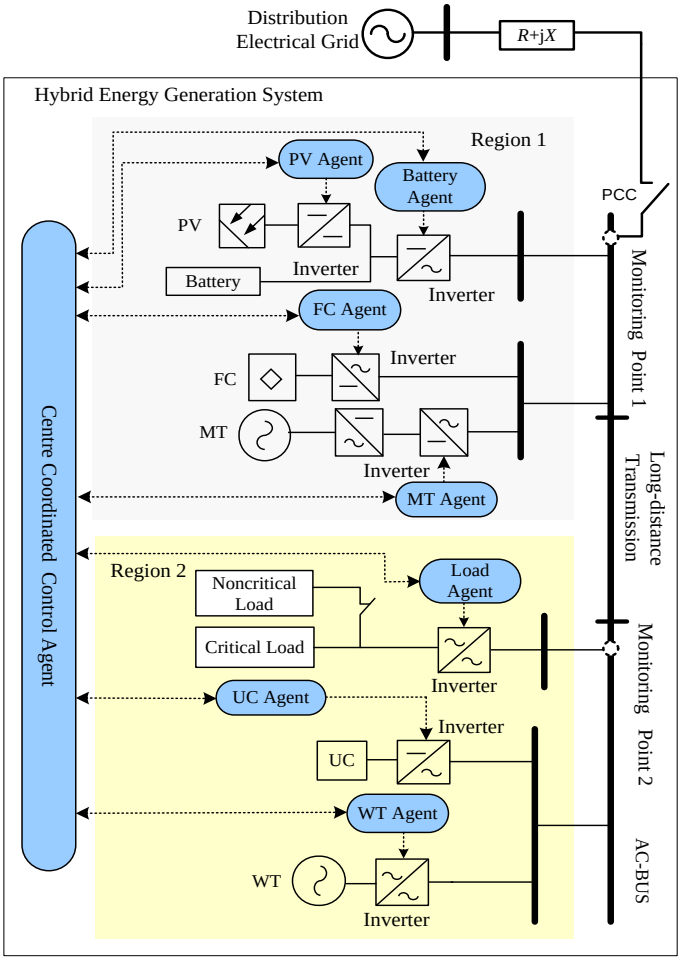

Fig. 1. MAS based control scheme of HEGS.

With respect to the grid-disconnected HEGS, the MAS is built with the following features: (i) in the lower level, seven unit agents are mainly responsible for ISCs and distributed dynamic regulation for its unit system; (ii) in the upper level, one CCCA implements CSCs; (iii) all agents interact each other according to the designed interactive modes.

Each lower-level unit agent is designed as hybrid agent, which is composed of *reactive* and *deliberative* layers as shown in Fig. 2. The *reactive* layer defined as "*recognition, perception and action*," has priority to respond quickly to the emergencies of operation status. The *deliberative* layer defined as "*belief, desire and intent*", has higher intelligence to control the hybrid behaviors of its unit system. The *belief* comes from environment recognition and knowledge base. The *desire* is to ensure security and dynamic performance of the unit system. The *intent* is to determent local hybrid controls including the ISC and the distributed dynamic control based on the current *belief* and *desire*. Finally, the local hybrid controls is executed by means of the action module. Notice that the time scale of the local hybrid controls is in the level of millisecond.

The upper-level CCCA is designed as a *belief-desire-intent* agent as shown in Fig. 3. The *belief* of the agent comes from the information exchanged between agents and knowledge base. The *desire* is to ensure security of the overall system. The *intent* is to determine the CSC based on the current *belief* and *desire* in decision-making module. Finally, the CSC is sent to corresponding unit agent by means of the action module. In this case, the time scale of the CSC is executed in the level of millisecond or second.

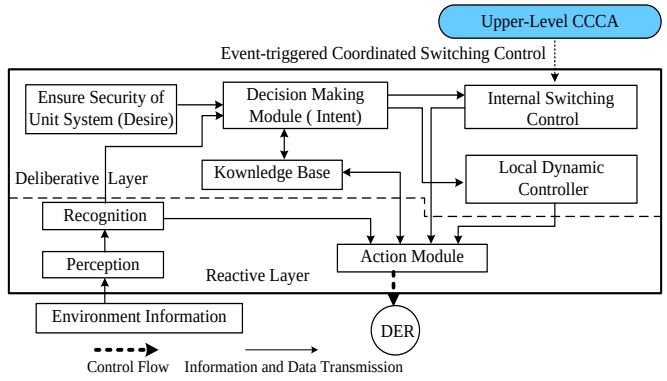

Fig. 2. Structure of the lower-level unit agent.

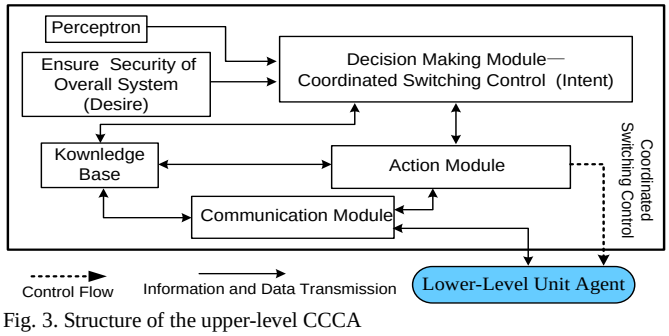

Fig. 3. Structure of the upper-level CCCA

In the MAS, the interactive modes between agents are designed as follows: (i) master-slave mode between the CCCA and the unit agents, which means that request of the upper-level CCCA must be responded by the asked lower-level unit agent; and (ii) non-master-slave modes between the unit agents, which implies that the lower-level unit agents interact in an equal way.

III. Event-triggered Hybrid Controls

It is well known that the DHPN model is one of the most useful modeling methods for complex hybrid systems [19], [20]. In order to fully describe the hybrid behaviors of DERs and the logical relationships between them, the DHPN modelling of the HEGS is firstly discussed.

A. DHPN Model of the HEGS

Corresponding to Fig. 1, DHPN model of the HEGS is built as shown in Fig.4. The DHPN model is defined by a 9-tuple (P_D, T_D, P_{DF}, T_{DF}, A_N, P_{re}, P_{os}, Γ, M_0) set, where

$P_D \in \{P_1, P_2, \ldots, P_{21}\}$ is a set of discrete places, which represents operation modes of all DER and load units;

$T_D \in \{T_1, T_2, \ldots, T_{34}\}$ is a set of discrete transitions, which represents event-triggered switching behaviors;

$P_{DF} \in \{P_{1f}, P_{2f}, \ldots, P_{7f}\}$ is a set of continuous places, which describes continuous dynamics of all unit systems;

$T_{DF} \in \{T_{1f}, T_{2f}, \ldots, T_{10f}\}$ is a set of continuous transitions, which represents distributed continuous controls of all unit systems;

$P = P_D \cup P_{DF}$, $T = T_D \cup T_{DF}$, $P \cap T = \phi$, $P \cup T \neq \phi$;

The detailed descriptions regarding places and transitions above are given in Tables I-IV in Appendix.

$A_N \subseteq ((P_D \times T_D) \cup (T_D \times P_D)) \cup ((P_D \times T_{DF}) \cup (T_{DF} \times P_D))$ is a set of arcs;

P_{re} is defined as predecessor function associated with the arc;

P_{os} is defines as posterior function associated with the arc;

Here, all the arc functions are defined as "1".

$\Gamma \in \{d_{T1}, d_{T2}, \ldots, d_{T34}, d_{T1f}, \ldots, d_{T10f}\}$ is a timing map for all the transients, which defines the triggered time of all the transients.

$M_0 \in \{M_{10}, M_{20}, \ldots, M_{70}\}$ is the initial marking of seven unit systems.

The initial operation mode of each unit system is marked with a token, which is described as discrete place with a black dot in Fig. 4. If the operation mode of a unit system is in P_i, then P_i is defined as logic "1", and accordingly other operation modes are certainly logic "0", since in each unit system, only one operation mode is "1". Therefore, corresponding to the DHPN model in Fig. 4, the initial markings of all unit systems are as follows.

Battery unit: $M_{10}(P_1, P_2, P_3, P_4, P_5)=[1,0,0,0,0]$;
PV unit: $M_{20}(P_6, P_7)=[1,0]$;
MT unit: $M_{30}(P_8, P_9)=[1,0]$;
FC unit: $M_{40}(P_{10}, P_{11})=[1,0]$;
Load unit: $M_{50}(P_{12}, P_{13})=[1,0]$;
UC unit: $M_{60}(P_{14}, P_{15}, P_{16}, P_{17}, P_{18})=[1,0,0,0,0]$;
WT unit: $M_{70}(P_{19}, P_{20}, P_{21})=[1,0,0]$.

The switching principle of the DHPN model is as follows: when one transition is triggered, if the predecessor place connected with the transition has token, then the token is transmitted into the posterior place connected with the transition, and accordingly resulting in switching of operation mode. In the light of the principle above, to switch the operation modes of all unit systems in a coordinated way, all transitions of the DHPN model should be triggered by means of designed logi-

cal control functions. Therefore, in this paper, the switching controls for operation mode are innovatively designed as the triggered functions of transitions.

In Fig. 4, the hierarchical event-triggered hybrid controls are described as follows: (i) The ISC in the lower-level unit agent, which is responsible for locally switching the operation mode of unit system, and described as "—▷"; (ii) The distributed dynamic control in the lower-level unit agent, which is responsible for the dynamic regulation of unit systems, and described as " ⇢ "; (iii) The CSC in the upper-level CCCA, which is responsible for switching operation modes of all unit systems in a coordinated way, and described as "→".

The rest of the paper is mainly focus on designing the event-triggered hybrid controls.

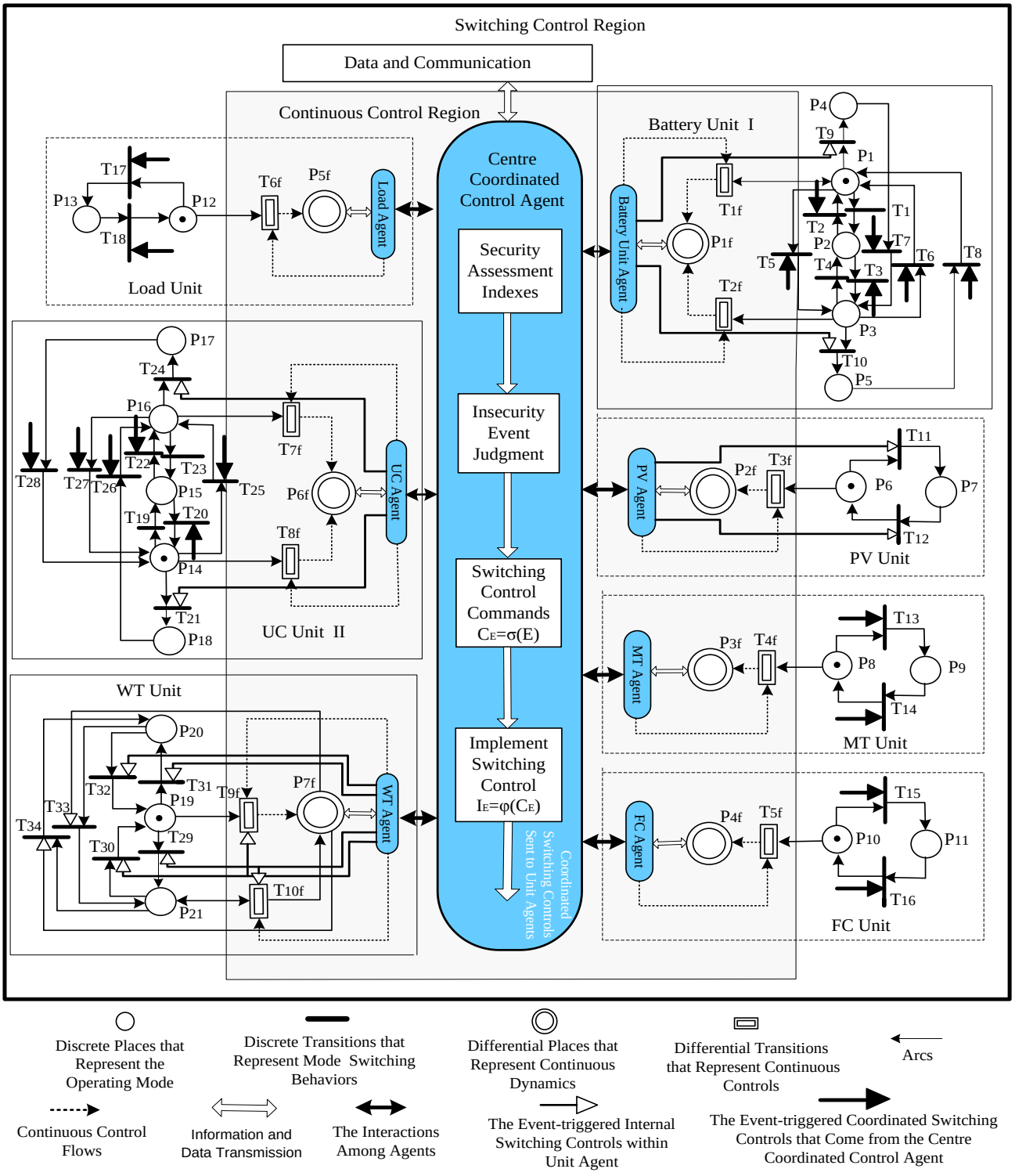

Fig. 4. Event-triggered hybrid controls based on the DHPN model

B. ISC

The ISC "⟶▷" is designed as a set of triggered functions of transitions, where CVFs are triggered conditions of them. The design concept is explained as follows: (i) once a constraint condition is violated, and correspondingly the designed CVF is activated (becomes logic "1"); (ii) it triggers the connected transition, according to the switching principle of the DHPN, corresponding operation mode can be switched.

In the PV unit, the ISCs are designed as follows

$$\text{If } t=t_0, \text{CVF: } G_{ing}(t) \text{ drops to } G_{\text{ing}}(t) \le C,$$
$$\text{then ISC}(T_{11}) = 1(t-t_0) - 1(t-t_0-d_{T11}) . \quad (1)$$

where $G_{ing}(t)$ is the incident irradiance; C is the threshold value; $1(t-t_0)$ is unit step function as

$$1(t-t_0) = \begin{cases} 1, & t \ge t_0 \\ 0. & t < t_0 \end{cases}.$$

The design of ISC(T_{11}) is explained as follows: at $t=t_0$, if $G_{ing}(t)$ drops to $G_{\text{ing}}(t) \le C$, and accordingly the CVF is activated, and then triggers the transition T_{11} for the duration time of d_{T11}, resulting in that operation mode of the PV unit is switched from P_6 to P_7. The following designs are in a similar way.

$$\text{If } t=t_0, \text{CVF: } G_{ing}(t) \text{ rises to } G_{\text{ing}}(t) > C,$$
$$\text{then ISC}(T_{12}) = 1(t-t_0) - 1(t-t_0-d_{T12}) . \quad (2)$$

In the WT unit, the ISCs are designed as follows

$$\text{If } t=t_0, \text{CVF: } v(t) \text{ drops to } v(t) \le v_{ci},$$
$$\text{then ISC}(T_{31}) = 1(t-t_0) - 1(t-t_0-d_{T31}) . \quad (3)$$
$$\text{If } t=t_0, \text{CVF: } v(t) \text{ rises to } v_{ci} < v(t) \le v_R,$$
$$\text{then ISC}(T_{32}) = 1(t-t_0) - 1(t-t_0-d_{T32}) . \quad (4)$$
$$\text{If } t=t_0, \text{CVF: } v(t) \text{ rises to } v_R < v(t) \le v_{co},$$
$$\text{then ISC}(T_{29}) = 1(t-t_0) - 1(t-t_0-d_{T29}) ,$$
$$\text{and ISC}(T_{10f}) = 1(t-t_0) - 1(t-t_0-d_{T10f}) . \quad (5)$$
$$\text{If } t=t_0, \text{CVF: } v(t) \text{ rises to } v(t) > v_{co},$$
$$\text{then ISC}(T_{34}) = 1(t-t_0) - 1(t-t_0-d_{T34}) . \quad (6)$$
$$\text{If } t=t_0, \text{CVF: } v(t) \text{ drops to } v_R < v(t) \le v_{co},$$
$$\text{then ISC}(T_{33}) = 1(t-t_0) - 1(t-t_0-d_{T33}) . \quad (7)$$
$$\text{If } t=t_0, \text{CVF: } v(t) \text{ drops to } v_{ci} < v(t) \le v_R$$
$$\text{then ISC}(T_{30}) = 1(t-t_0) - 1(t-t_0-d_{T30}) ,$$
$$\text{and ISC}(T_{9f}) = 1(t-t_0) - 1(t-t_0-d_{T9f}) . \quad (8)$$

where $v(t)$ is the wind speed; v_{ci} is the cut-in wind speed; v_{co} is the cut-off wind speed; v_R is the rated wind speed.

In the battery unit, the ISCs are designed as follows

$$\text{If } t=t_0, \text{CVF: SOC}(t) \text{ drops to SOC}(t) \le \text{SOC}_{\min},$$
$$\text{then ISC}(T_9) = 1(t-t_0) - 1(t-t_0-d_{T9}) , \quad (9)$$
$$\text{If } t=t_0, \text{CVF: SOC}(t) \text{ rises to SOC}(t) \ge \text{SOC}_{\max},$$
$$\text{then ISC}(T_{10}) = 1(t-t_0) - 1(t-t_0-d_{T10}) , \quad (10)$$

where SOC(t) is the state of charge; $\text{SOC}_{\max}$ and $\text{SOC}_{\min}$ are the maximum and minimum values, respectively.

In the UC unit, the ISCs are designed as follows

$$\text{If } t=t_0, \text{CVF: } U(t) \text{ drops to } U(t) \le U_{\min},$$
$$\text{then ISC}(T_{21}) = 1(t-t_0) - 1(t-t_0-d_{T21}) , \quad (11)$$
$$\text{If } t=t_0, \text{CVF: } U(t) \text{ rises to } U(t) \ge U_{\max},$$
$$\text{then ISC}(T_{24}) = 1(t-t_0) - 1(t-t_0-d_{T24}) , \quad (12)$$

where $U(t)$ is the voltage of the UC; $U_{\max}$ and $U_{\min}$ are the maximum and minimum values of $U(t)$, respectively.

C. Distributed Dynamic Control

In different operation mode (except stopping mode), each unit system is regulated in a distributed way by using different dynamic control strategies [21]-[23]. In the HEGS, the storage unit is regarded as a grid-forming control unit, which is mainly responsible for the frequency/voltage (*f-V*) regulations by means of *f-V* droop control strategies as shown in Fig. 5. Other DER units like FC/MT, PV and WT, are defined as grid-following control units, which is mainly responsible for a desired amount of active/reactive output powers by means of *P-Q* control strategies as shown in Fig. 6.

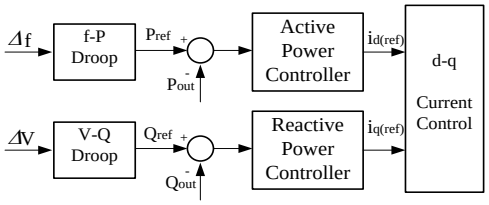

Fig. 5. Grid-forming *f-V* droop control strategy

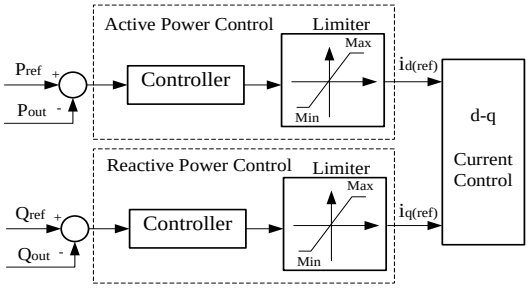

Fig. 6. Grid-following *P-Q* control strategy

With respect to two kinds of control strategies above, outer-loop active/reactive power controllers are designed based on different droop characteristics to achieve different control objectives, and inner-loop voltage/current controllers are designed as H∞ robust controllers instead of traditional PI controllers to enhance capacity of resisting disturbance. The detailed design regarding the two loops of controllers had been presented in author's previous research [24]. Considering the limitation of paper pages, the design process is here not presented again.

D. CSC

The CSC "⟶" is also designed as a set of triggered functions of transitions, where voltage SAIs are triggered conditions of them. The design concept is explained as follows: (i) once a voltage SAI exceeds the desired secure range, correspondingly an insecure event is estimated to occur, and then its event-triggered function is activated (becomes logic "1"); (ii) it triggers the connected transition, according to the switching principle of the DHPN, corresponding operation mode can be switched. The CSC is design according to the following steps.

Step 1: SAIs

The insecure voltage generally is manifested initially as a slow voltage decay following a sharp decline at the point of collapse. Therefore, the voltage magnitude alone cannot be regarded as a reliable SAI. In this paper, dynamic voltage SAIs are constructed by using the voltage sequences at two monitoring points, which are set at PCC and load nodes in two regions [25].

The voltage sequences at the two monitoring points are represented as $V_i = [V_i^1, V_i^2, ..., V_i^N], i \in 1,2.$

(i) The moving average voltage values at the *i*-th node at the *t*-th instant are obtained by using *N* available voltage measurements

$$V_i^{(t)} = \sum_{k=1}^{t} V_i^k / t \quad t \in 1,2,\cdots,N; \quad if\ t \le N;$$

$$V_i^{(t)} = \sum_{k=t-N+1}^{t} V_i^k / N \quad t \in N+1, N+2,\cdots,m; \quad if\ t > N. \quad (13)$$

(ii) The percentages of diversity between the real voltage V_i^t and moving average value $V_i^{(t)}$ at the *t*-th instant are defined as

$$C_i^t = \frac{V_i^t - V_i^{(t)}}{V_i^{(t)}} \times 100, t \in 1,2,\cdots,m. \quad (14)$$

(iii) The voltage SAIs at the *t*-th instant are estimated by dividing the area under the percentage of diversity curve

$$U_i^{(t)} = \sum_{k=1}^{t} (C_i^k + C_i^{k-1})/2t \quad t \in 1,2,\cdots,N; \quad if\ t \le N;$$

$$U_i^{(t)} = \sum_{k=t-N+1}^{t} (C_i^k + C_i^{k-1})/2N,$$

$$t \in N+1, N+2,\cdots,m; \quad if\ t > N. \quad (15)$$

Step 2: Insecure event judgment

By means of the voltage SAIs above, insecure events are judged as follows.

(i) Define the voltage SAI at the *t*-th instant at the PCC node as $U_1^{(t)}$, and at the load node as $U_2^{(t)}$.

(ii) Set the maximum and maximum thresholds of the voltage SAI at the PCC node as $U_{1\max}$ and $U_{1\min}$, and at the load node as $U_{2\max}$ and $U_{2\min}$.

(iii) At the *t*-th instant,

when $U_1^{(t)} > U_{1\max}$, define that the event $E_{11}(t)$ occurs;

when $U_1^{(t)} < U_{1\min}$, define that the event $E_{12}(t)$ occurs;

when $U_2^{(t)} > U_{2\max}$, define that the event $E_{21}(t)$ occurs;

when $U_2^{(t)} < U_{2\min}$, define that the event $E_{22}(t)$ occurs.

(iv) In this paper, we set two voltage monitoring points in two regions, according to the above definitions, at the *t*-th instant, there are potentially six kind of insecure events at least as follows

$E_1(t)=\{E_{11}(t)\}$; $E_2(t)=\{E_{12}(t)\}$; $E_3(t)=\{E_{21}(t)\}$,

$E_4(t)=\{E_{22}(t)\}$; $E_5(t)=\{E_{11}(t),E_{21}(t)\}$; $E_6(t)=\{E_{21}(t), E_{22}(t)\}$.

Step 3: CSCs

Before design the CSCs, we define the following logic relation and switching principle:

(i) If at the *t*-th instant, E_1 insecure event is judged to occur, then $E_1(t)$ is activated and becomes logic "1"; otherwise, $E_1(t)$ is logic "0";

(ii) Each CSC is activated no more than three times.

At the $t = t_0$ instant, corresponding to the above six kinds of insecure events, the CSCs are designed as follows.

$$\begin{aligned}
C(E_1) = {} & E_1(t)\{P_1(1(t-t_0)-1(t-t_0-d_{T5}))+P_2(1(t-t_0)-1(t-t_0-d_{T3}) \\
& +P_4(1(t-t_0)-1(t-t_0-d_{T7}))\} \\
& +E_1(t+\Delta t)\{P_8(1(t-t_0-\Delta t)-1(t-t_0-\Delta t-d_{T13})) \\
& +P_{10}(1(t-t_0-\Delta t)-1(t-t_0-\Delta t-d_{T15}))\} \\
& +E_1(t+2\Delta t)\{P_{14}(1(t-t_0-2\Delta t)-1(t-t_0-2\Delta t-d_{T25})) \\
& +P_{15}(1(t-t_0-2\Delta t)-1(t-t_0-2\Delta t-d_{T22}))\}
\end{aligned}$$

$$\begin{aligned}
C(E_2) = {} & E_2(t)\{P_3(1(t-t_0)-1(t-t_0-d_{T6}))+P_2(1(t-t_0)-1(t-t_0-d_{T2})) \\
& +P_5(1(t-t_0)-1(t-t_0-d_{T8}))\} \\
& +E_2(t+\Delta t)\{P_9(1(t-t_0-\Delta t)-1(t-t_0-\Delta t-d_{T14})) \\
& +P_{11}(1(t-t_0-\Delta t)-1(t-t_0-\Delta t-d_{T16}))\} \\
& +E_2(t+2\Delta t)\{P_{16}(1(t-t_0-2\Delta t)-1(t-t_0-2\Delta t-d_{T27})) \\
& +P_{15}(1(t-t_0-2\Delta t)-1(t-t_0-2\Delta t-d_{T20})) \\
& +P_{17}(1(t-t_0-2\Delta t)-1(t-t_0-2\Delta t-d_{T28}))\} \quad (17)
\end{aligned}$$

$$\begin{aligned}
C(E_3) = {} & E_3(t)\{P_{14}(1(t-t_0)-1(t-t_0-d_{T25}))+P_{15}(1(t-t_0)-1(t-t_0-d_{T22})) \\
& +P_{18}(1(t-t_0)-1(t-t_0-d_{T26}))\} \\
& +E_3(t+\Delta t)\{P_1(1(t-t_0-\Delta t)-1(t-t_0-\Delta t-d_{T5})) \\
& +P_2(1(t-t_0-\Delta t)-1(t-t_0-\Delta t-d_{T3})) \\
& +P_4(1(t-t_0-\Delta t)-1(t-t_0-\Delta t-d_{T7}))\} \\
& +E_3(t+2\Delta t)\{P_8(1(t-t_0-2\Delta t)-1(t-t_0-2\Delta t-d_{T13})) \\
& +P_{10}(1(t-t_0-2\Delta t)-1(t-t_0-2\Delta t-d_{T15}))\} \quad (18)
\end{aligned}$$

$$\begin{aligned}
C(E_4) = {} & E_4(t)\{P_{15}(1(t-t_0)-1(t-t_0-d_{T20}))+P_{16}(1(t-t_0)-1(t-t_0-d_{T27})) \\
& +P_{17}(1(t-t_0)-1(t-t_0-d_{T28}))\} \\
& +E_4(t+\Delta t)\{P_2(1(t-t_0-\Delta t)-1(t-t_0-\Delta t-d_{T2})) \\
& +P_3(1(t-t_0-\Delta t)-1(t-t_0-\Delta t-d_{T6})) \\
& +P_5(1(t-t_0-\Delta t)-1(t-t_0-\Delta t-d_{T8}))\} \\
& +E_4(t+2\Delta t)\{P_9(1(t-t_0-2\Delta t)-1(t-t_0-2\Delta t-d_{T14})) \\
& +P_{11}(1(t-t_0-2\Delta t)-1(t-t_0-2\Delta t-d_{T16}))\} \quad (19)
\end{aligned}$$

$$\begin{aligned}
C(E_5) = {} & E_5(t)\{P_{13}(1(t-t_0)-1(t-t_0-d_{T18}))\} \\
& +E_5(t+\Delta t)\{P_1(1(t-t_0-\Delta t)-1(t-t_0-\Delta t-d_{T5})) \\
& +P_2(1(t-t_0-\Delta t)-1(t-t_0-\Delta t-d_{T3})) \\
& +P_4(1(t-t_0-\Delta t)-1(t-t_0-\Delta t-d_{T7}))\} \\
& +E_5(t+\Delta t)\{P_{14}(1(t-t_0-\Delta t)-1(t-t_0-\Delta t-d_{T25})) \\
& +P_{15}(1(t-t_0-\Delta t)-1(t-t_0-\Delta t-d_{T22})) \\
& +P_{18}(1(t-t_0-\Delta t)-1(t-t_0-\Delta t-d_{T26}))\} \\
& +E_5(t+2\Delta t)\{P_8(1(t-t_0-2\Delta t)-1(t-t_0-2\Delta t-d_{T13})) \\
& +P_{10}(1(t-t_0-2\Delta t)-1(t-t_0-2\Delta t-d_{T15}))\} \quad (20)
\end{aligned}$$

$$\begin{aligned}
C(E_6) = {} & E_6(t)\{P_3(1(t-t_0)-1(t-t_0-d_{T6}))+P_2(1(t-t_0)-1(t-t_0-d_{T2})) \\
& +P_5(1(t-t_0)-1(t-t_0-d_{T8}))\} \\
& +E_6(t)\{P_{16}(1(t-t_0)-1(t-t_0-d_{T27}))+P_{15}(1(t-t_0)-1(t-t_0-d_{T20})) \\
& +P_{17}(1(t-t_0)-1(t-t_0-d_{T28}))\} \\
& +E_6(t+\Delta t)\{P_9(1(t-t_0-\Delta t)-1(t-t_0-\Delta t-d_{T14})) \\
& +P_{11}(1(t-t_0-\Delta t)-1(t-t_0-\Delta t-d_{T16}))\} \\
& +E_6(t+2\Delta t)\{P_{12}(1(t-t_0-2\Delta t)-1(t-t_0-2\Delta t-d_{T17})) \quad (21)
\end{aligned}$$

where, $C(E_i)$ represents the CSC of $E_i(t)$, $i \in \{1,2,\cdots,6\}$, and Δt is switching interval.

Take $C(E_1)$ in (16) as an example, the design is explained as follows: (i) when $t = t_0$, if the insecure event E_1 is judged to occur, and at that moment the battery unit runs in any one of P_1, P_2 and P_4 modes, then $C(E_1)$ is activated to become "logic 1". (ii) After the time of Δt, if the event E_1 still exists, and at the moment the MT and FC units respectively runs in P_8 and P_{10} modes, then the $C(E_1)$ is activated again. (iii) After the time of $2\Delta t$, if the event E_1 still exists, and at the moment the UC unit runs in any one of P_{15} and P_{18} modes, then the

C(E1) is activated again.

The process above implies that, (i) the times of activation of CSC is no more than three times; (ii) the time interval of activation is Δt; (iii) the switching sequence is from the battery to FC/MT to UC unit; and (iv) the duration time of activation is set according to the requirement of switching time of different operation mode. For example, when the battery is in P1, the duration time of activation of C(E1) is d_{T5}; while when the battery is in P2, the duration time of activation of C(E1) is d_{T3},

The rest of CSCs are explained in a similar way.

Step 4: Implementation of CSC

The above CSCs need to be sent to corresponding unit agents by the CCCA, and are applied to corresponding transitions, and accordingly resulting in switching of operation modes. Implementation strategies of CSCs are designed as follows.

$$I_{E1}(T_5)=I_{E1}(T_3)=I_{E1}(T_7)=I_{E1}(T_{13})=I_{E1}(T_{15}) =I_{E1}(T_{25})=I_{E1}(T_{22})=I_{E1}(T_{26})=C(E_1) \quad (22)$$

$$I_{E2}(T_6)=I_{E2}(T_2)=I_{E2}(T_8)=I_{E2}(T_{14})=I_{E2}(T_{16}) =I_{E2}(T_{27})=I_{E2}(T_{20})=I_{E2}(T_{28})=C(E_2) \quad (23)$$

$$I_{E3}(T_{25})=I_{E3}(T_{22})=I_{E3}(T_{26})=I_{E3}(T_5)=I_{E3}(T_3) =I_{E3}(T_7)=I_{E3}(T_{13})=I_{E3}(T_{15})=C(E_3) \quad (24)$$

$$I_{E4}(T_{20})=I_{E4}(T_{27})=I_{E4}(T_{28})=I_{E4}(T_2)=I_{E4}(T_6) =I_{E4}(T_8)=I_{E4}(T_{14})=I_{E4}(T_{16})=C(E_4) \quad (25)$$

$$I_{E5}(T_{18})=I_{E5}(T_5)=I_{E5}(T_3)=I_{E5}(T_7)=I_{E5}(T_{25}) =I_{E5}(T_{22})=I_{E5}(T_{26})=I_{E5}(T_{13}) =I_{E5}(T_{15})=C(E_5) \quad (26)$$

$$I_{E6}(T_6)=I_{E6}(T_2)=I_{E6}(T_8)=I_{E6}(T_{27})=I_{E6}(T_{20}) =I_{E6}(T_{28})=I_{E6}(T_{14})=I_{E6}(T_{16}) =I_{E6}(T_{17})=C(E_6) \quad (27)$$

where, $I_{E1}(T_5)$ represents event-triggered function of transition T_5 when the event E_1 is judged to occur. The rest is defined in a similar way.

Take the design of (22) as an example, which is explained as follows: when $t=t_0$, the insecure event E1 is judged to occur, and the C(E1) is sent to the battery, MT/FC and UC unit agents by the CCCA. Then, it trigger transitions T_5, T_3, T_7, T_{13}, T_{15}, T_{25}, T_{22} and T_{26} according to different activation sequence of C(E1), so that corresponding operation modes can be switched in proper order to guarantee power supply in a high-security level. The rest of event-trigged functions are done in a similar way.

IV. Simulation Results

In order to verify the validity of proposed approach, the HEGS as shown in Fig. 1, was simulated on a typical day from 8 to 24 o'clock.

Case 1: Load following

The critical and noncritical load demands are shown in Fig.7(a), and wind speed and sun irradiance are given in Fig.7(b). By means of the proposed MAS based hybrid controls, the active powers of the six DER units are given in Fig. 7(c). Moreover, the proposed approach is compared with three switching control schemes: (i) the logical judgment that is similar to [14]; (ii) the fuzzy-logical-rule that is similar to [15]; and (iii) the authors' previous research [16]. The comparative results are presented in terms of the voltage control performance at the PCC and load nodes as shown in Figs. 7(d) and (e).

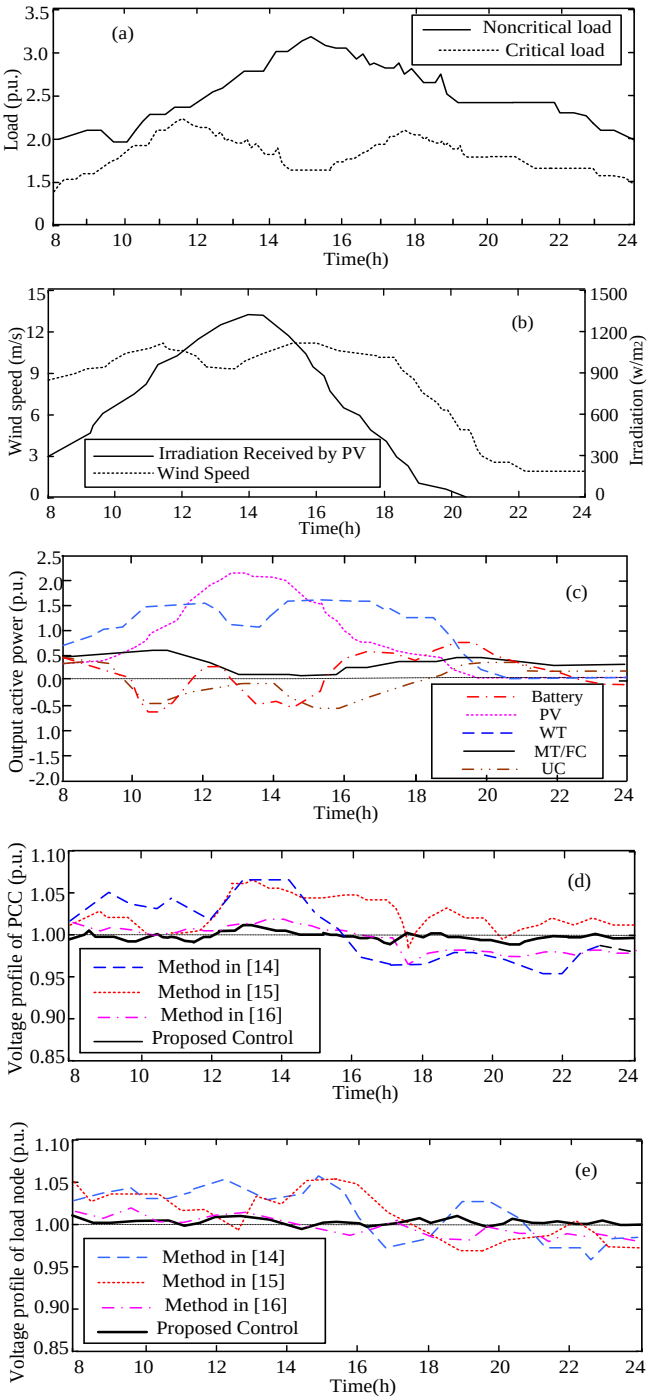

Fig. 7. Control performance in the case I.
(a) curves of loads; (b) wind speed and sun irradiance; (c) active powers all DER units; (d) voltage profile on PCC node; (e) voltage profile on load node.

By using the proposed MAS based hybrid controls, the controllable DER units operation modes are switched as shown in Fig.8.

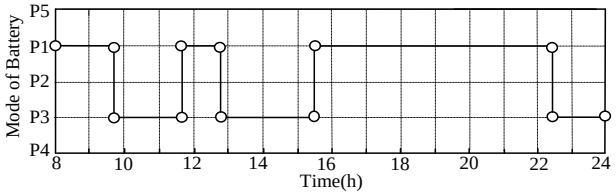

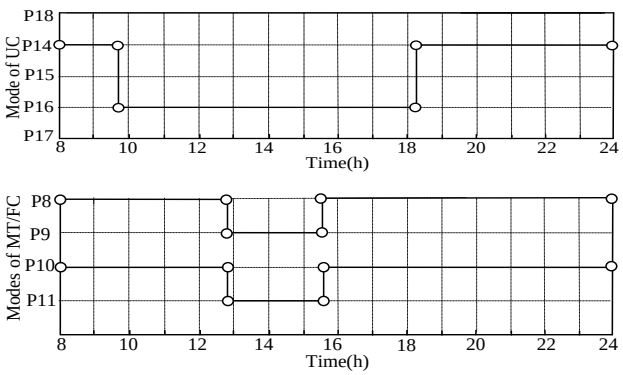

Fig.8. Operation modes of four controllable DER units.

From Figs. 7(c) and 8, it can be seen that the operation of controllable DER units are switched by means of the CSCs as shown in Table V.

TABLE V. OPERATION MODE SWITCHING BE MEANS OF THE CSCS

Orders	Times	Insecure Events	Operation mode switching
(1)	9.40	E_5	The transition T_{25} is triggered so that the UC unit is switched from discharging to charging mode. After one switching interval time, T_5 is triggered so that battery unit is switched from the discharging to the charging mode.
(2)	11.40	E_2	The transition T_6 is triggered so that the battery unit is switched from the charging to the discharging mode.
(3)	12.45	E_1	The transition T_5 is triggered so that the battery unit is switched from the discharging to the charging mode. After one switching interval time, T_{13} and T_{15} are triggered simultaneously so that the FC&MT units are switched from the rated operation to the low-output operation mode.
(4)	15.30	E_2	The transition T_6 is triggered so that the battery unit is switched from the charging to the discharging mode. After one switching interval time, T_{14} and T_{16} are triggered simultaneously so that the FC&MT units are switched from the low-output operation to the rated operation mode.
(5)	18.15	E_4	The transition T_{27} is triggered so that the UC unit is switched from the charging mode to the discharging mode.

From Figs. 7(d) and (e), it can be shown that by means of the first two schemes, the PCC and load voltages are not controlled within the secure range of 0.95p.u. to 1.05p.u. The reason is that, only by switching the operation modes of the storage units, the unbalanced power cannot be regulated quickly, and thus resulting in larger voltage fluctuations. By using the authors' previous control scheme in [16], the PCC and load voltages can be maintained within the secure range. However, in comparison with the voltage performance obtained by using the proposed hybrid controls in this paper, they present a bit larger fluctuations. The above simulation results show that the proposed MAS based hybrid controls can meet changed loads with the best voltage performance.

Case II: Load disturbance

At 11.40am the critical load increases 50 percent as shows in Fig. 9(a). Fig. 9(b) shows the active powers of all DER units by using the proposed hybrid controls. Specially at 11.40am, the insecurity event E_6 is estimated to occur, and accordingly the triggered function $C(E_6)$ is activated, and then triggers the transitions T_{27} and T_6 simultaneously, so that the UC and battery units are switched from the charging to discharging mode. By means of the CSCs above, the PCC and load voltages can return to the normal range rapidly. Therefore, from Fig.9(c) and (d), it can be seen that, by using the proposed control even if at the 11:40am, the sudden load increase does not lead to severe decline of the voltage. The PCC and load voltages can be regulated rapidly within the range of 0.98p.u.to 1.02p.u. From Fig.9(c) and (d), it can be also shown that by means of control schemes in [14] and [15], at 11:40am the sudden load increase results in sharp voltage drops, afterwards these voltages present larger fluctuations. The reason is that, in [14] and [15] the switching control is only applied to the storage units, and thus the unbalance between supply and demand cannot be regulated enough quickly. In addition, in comparison with the proposed control, the voltage performance by using the control scheme in [18] is a little bit worse. The simulation results show that the proposed MAS based hybrid controls can ensure the best voltage performance when faced with a large load disturbance.

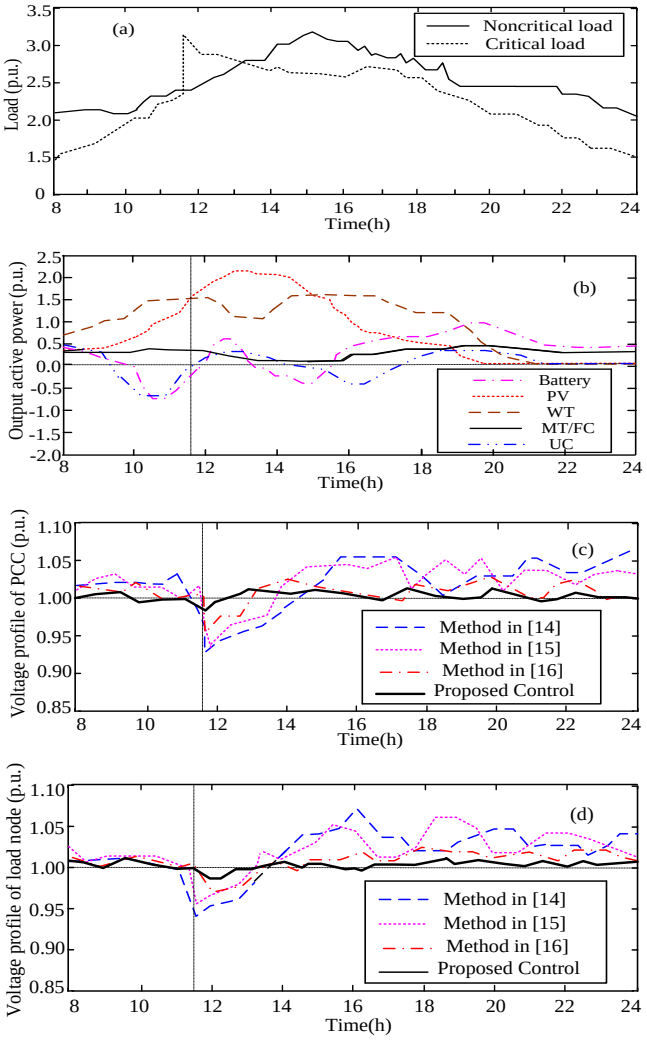

Fig. 9. Control performance in the case II.
(a) curves of loads; (b) active powers all DER units; (c) voltage profile at PCC node; (d) voltage profile at load node.

V. Conclusion

This paper proposes MAS based event-triggered hybrid controls, by which the HEGS can ensure energy supply with high security. As original works, the hierarchical hybrid controls are designed with taking full consideration of the hybrid behaviors of all DERs, and then is implemented be means of the MASs in a distributed coordinated way. In comparison with the simulation results of pervious relevant researches, the proposed hybrid controls present the best voltage performance.

The proposed MAS based hybrid controls only relies on sparse communication network. Despite the upper-level CCCA needs to know the operation modes of all unit systems, the information can be obtained through both direct and indirect interactions between agents. Therefore, the proposed scheme does not require a fully connected communication network throughout the HEGS.

In addition, the proposed scheme can be easily extended for controlling other energy networks, such as active distribution grids and smart grids, by changing the switching controls according to different logic relationships between DER units, developing the function of agents and creating additional agents.

References

[1] S. M. Ashabani, and Y. A. I. Mohamed, "New family of Microgrid control and management strategies in smart distribution grids—analysis, comparison and testing," *IEEE Transactions on Power Systems*, vol. 29, no.5, pp. 2257-2269, 2014.

[2] A. Khodaei, "Provisional Microgrids," *IEEE Transactions on Smart Grid*, vol. 6, no. 3, pp. 1107-1115, 2015.

[3] J. Guerrero, M. Chandorkar, T. Lee, and P. Loh, "Advanced control architectures for intelligent microgrids—Part I: Decentralized and hierarchical control," *IEEE Transactions on Industrial Electronics*, vol. 60, no. 4, pp. 1254-1262, 2013.

[4] A. Bidram, and A. Davoudi, "Hierarchical structure of microgrids control system," *IEEE Transactions on Smart Grid*, vol. 3, no. 4, pp. 1963-1976, 2012.

[5] E. M. Natsheh, A. R. Natsheh and A. Albarbar, "Intelligent controller for managing power flow within standalone hybrid power systems," *IET Science, Measurement and Technology*, vol. 7, no. 4, pp. 191-200, 2013.

[6] Q. Li, W. R. Chen, Y. K. Li, S. K. Liu, and J. Huang, "Energy management strategy for fuel cell/battery/ultracapacitor hybrid vehicle based on fuzzy logic," *Electrical Power and Energy Systems*, vol. 43, pp. 514-525, 2012.

[7] A. Kaabeche, and R. Ibtiouen, "Techno-economic optimization of hybrid photovoltaic/wind/diesel/battery generation in a stand-alone power system," *Solar Energy*, vol. 103, pp. 171-182, 2014.

[8] A. Ghazanfari, M. Hamzeh, H. Mokhtari, and H. Karimi, "Active power management of multihybrid fuel cell/supercapacitor power conversion system in a medium voltage Microgrid," *IEEE Transactions on Smart Grid*, vol. 3, no. 4, pp.1903-1910, 2012.

[9] Z. H. Jiang, L. J. Gao, and R. A. Dougal, "Adaptive control strategy for active power sharing in hybrid fuel cell/battery power sources," *IEEE Transactions on Energy Conversion*, vol. 22, pp. 183-194, 2007.

[10] C. X. Dou, D. L. Liu, X. B. Jia, and F. Zhao, "Management and control for smart microgrid based on hybrid control theory," *Electric Power Components and Systems*, vol. 39, pp. 813-832, 2011.

[11] M. Tahir, and S. K. Mazumder, "Self-triggered communication enabled control of distributed generation in microgrids," *IEEE Transactions on Industrial Informatics*, vol. 11, no. 2, pp. 441-448, 2015.

[12] T. Logenthiran, D. Srinivasan, and A. M. Khambadkone, "Multi-agent system for energy resource scheduling of integrated microgrids in a distributed system," *Electric Power System Research*, vol. 81, No. 1, pp. 138-148, 2011.

[13] J. Zeng, J. F. Liu, J. Wu, and H. W. Ngan, "A multi-agent solution to energy management in hybrid renewable energy generation system," *Renewable Energy*, vol. 36, pp. 1352-1362, 2011.

[14] J. Lagorse, D. Paire, and A. Miraoui, "A multi-agent system for energy management of distributed power sources," *Renewable Energy*, vol. 35, pp. 174-182, 2010.

[15] J. Lagorse, M. G. Simoes, and A. Miraoui, "A multiagent fuzzy-logic-based energy management of hybrid systems," *IEEE Transactions on Industry Applications*, vol. 45, pp. 2123-2129, 2009.

[16] C.X. Dou, B. Liu, and J. M. Guerrero, "Event-triggered hybrid control based on multi-agent system for microgrids," *IET Generation, Transmission & Distribution*, vol.12, pp. 1987-1997, 2014.

[17] C. J. Li, X. H. Yu, W. W. Yu, T. W. Huang, and Z.W Liu, "Distributed event-triggered scheme for economic dispatch in smart grids" *IEEE Transactions on Industrial informatics*, DOI10.1109/TII.2015.2479558.

[18] S. P. Wen, X. H. Yu, Z. G. Zeng, and J. J. Wang, "Event-triggering load frequency control for multi-area power systems with communication delays" *IEEE Transactions on Industrial Electronics*, vol. 63, no. 2, pp. 1308-1317, 2016.

[19] H. Motallebi, and M. A. Azgomi, "Modeling and verification of hybrid dynamic systems using multisingular hybrid Petri nets," *Theoretical Computer Science*, vol. 446, pp. 48-74, 2012.

[20] H. C. Guo, G. Q. Li, and T. Li, "Analysis of gearbox fault diagnosis system of wind turbine based on fuzzy Petri nets," *In Conference on Fuzzy Systems and Knowledge Discovery*, pp.540-544, 2012

[21] W. Yao,M. Chen, J. Matas, J. M. Guerrero, and Z. Qian, "Design and analysis of the droop control method for parallel inverters considering the impact of the complex impedance on the power sharing," *IEEE Transactions on Industrial Electronics*, vol. 58, pp. 576-588, 2011.

[22] J. M. Guerrero, J. C. Vasquez, and J. Matas, "Hierarchical control of droop-controlled AC and DC microgrids—a general approach toward standardization," *IEEE Transactions on Industrial Electronics*, vol. 58, no.1, pp.158-172, 2011.

[23] B, Bahrani, and M, Saeedifard , "A multivariable design methodology for voltage control of a single-DG-unit microgrid," *IEEE Transactions on Industrial informatics*, vol. 9, no. 2, pp. 589-598, 2013.

[24] C. X. Dou, B. Liu, and D. J Hill, "Hybrid control for high-penetration distribution grid based on operational mode conversion," *IET Generation, Transmission & Distribution*, vol.7, no.7, pp.700-708, 2013.

[25] K. Seethalekshmi, S. N. Singh, and S. C. Srivastava, "A synchrophasor assisted frequency and voltage stability based load shedding scheme for self-healing of power system," *IEEE Transactions on Smart Grid*, vol. 2, pp. 221-230, 2011.

Appendix

Table I. Description Of Discrete Places

Discrete Places	Description
P_1	Discharging mode of the battery unit
P_2	Stopping mode with normal State of Charge (SOC) of the battery unit
P_3	Charging mode of the battery unit
P_4	Stopping mode with minimal SOC of the battery unit
P_5	Stopping mode with maximal SOC of the battery unit
P_6	Maximum Power Point Tracking (MPPT) mode of the PV unit
P_7	Stopping mode of the PV unit
P_8	Rated operation mode of the MT unit
P_9	Low-output operation mode of the MT unit
P_{10}	Rated operation mode of the FC unit
P_{11}	Low-output operation mode of the FC unit
P_{12}	Normal operation mode of the load unit
P_{13}	Shedding load operation mode of the load unit
P_{14}	Discharging mode of the UC unit
P_{15}	Stopping mode with normal voltage of the UC unit
P_{16}	Charging mode of the UC unit
P_{17}	Stopping mode with maximal voltage of the UC unit
P_{18}	Stopping mode with minimal voltage of the UC unit
P_{19}	MPPT operation mode of the WT unit
P_{20}	Stopping mode of the WT unit
P_{21}	Constant power output operation mode of the WT unit

Table II. Description Of Discrete Transitions

Discrete Transition	Description
T_1	Switch the battery unit from discharging mode to stopping mode with the normal SOC

T_2	Switch the battery unit from stopping mode with the normal SOC to discharging mode
T_3	Switch the battery unit from stopping mode with the normal SOC to charging mode
T_4	Switch the battery unit from charging mode to stopping mode with the normal SOC
T_5	Switch the battery unit from discharging mode to charge mode
T_6	Switch the battery unit from charging mode to discharge mode
T_7	Switch the battery unit from stopping mode with minimal SOC to charge mode
T_8	Switch the battery unit from stopping mode with maximal SOC to discharge mode
T_9	Switch the battery unit to stopping mode because SOC reaches to the minimum
T_{10}	Switch the battery unit to stopping mode because SOC reaches to the maximum
T_{11}	Switch the PV unit from MPPT mode to stopping mode
T_{12}	Switch the PV unit from stopping mode to MPPT mode
T_{13}	Switch the MT unit from rated mode to low-output mode
T_{14}	Switch the MT unit from low-output mode to rated mode
T_{15}	Switch the FC unit from rated mode to low-output mode
T_{16}	Switch the FC unit from low-output mode to rated mode
T_{17}	Switch the load unit from normal mode to shedding load mode
T_{18}	Switch the load unit from shedding load mode to normal mode
T_{19}	Switch the UC unit from discharging mode to stopping mode with the normal voltage
T_{20}	Switch the UC unit from stopping mode with the normal voltage to discharging mode
T_{21}	Switch the UC unit to stopping mode because the voltage reaches to the minimum
T_{22}	Switch the UC unit from stopping mode with the normal voltage to charging mode
T_{23}	Switch the UC unit from charging mode to stopping mode with the normal voltage
T_{24}	Switch the UC unit to stopping mode because the voltage reaches to the maximum
T_{25}	Switch the UC unit from discharging mode to charge mode
T_{26}	Switch the UC unit from stopping mode with minimal voltage to charge mode
T_{27}	Switch the UC unit from charging mode to discharge mode
T_{28}	Switch the UC unit from stopping mode with maximal voltage to discharge mode
T_{29}	Switch the WT unit from MPPT mode to constant output mode
T_{30}	Switch the WT unit from constant output mode to MPPT mode
T_{31}	Switch the WT unit from MPPT mode to stopping mode
T_{32}	Switch the WT unit from stopping mode to MPPT mode
T_{33}	Switch the WT unit from stopping mode to constant output mode
T_{34}	Switch the WT unit from constant output mode to stopping mode

TABLE III. DESCRIPTION OF DIFFERENTIAL PLACES

Differential Places	Description
P_{1f} -P_{10f}	Continuous dynamics of the corresponding units

TABLE IV. DESCRIPTION OF DIFFERENTIAL TRANSITIONS

Differential Transitions	Description
T_{1f} andT_{2f}	Dynamic controls of the battery unit in discharge and charge mode respectively
T_{3f}	Dynamic control of the PV unit in MPPT mode
T_{4f} and T_{5f}	Dynamic controls of the MT and FC units respectively in rated mode
T_{6f}	Dynamic control of the load unit in normal mode
T_{7f} andT_{8f}	Dynamic controls of the UC unit in charge and discharge mode respectively
T_{9f} andT_{10f}	Dynamic controls of the WT unit in MPPT and constant power output mode respectively

Chunxia Dou received the B.S. and M.S. degrees in automation from the Northeast Heavy Machinery Institute, Qiqihaer, China, in 1989 and 1994, respectively, and the Ph.D. degree in Institute of Electrical Engineering from Yanshan University, Qinhuangdao, China, in 2005. In 2010, he joined the Department of Engineering, Peking University, Beijing, China, where he was a Postdoctoral Fellow for two years. Since 2005, he has been a Professor in Institute of Electrical Engineering, Yanshan University. Her current research interests include multi-agent based control, event-triggered hybrid control, distributed coordinated control, and multi-mode switching control and their applications in power systems, Microgrids and smart grids.

Dong Yue (SM'08) received the Ph.D. degree from the South China University of Technology, Guangzhou, China, in 1995. He is currently a professor and dean of Institute of Advanced Technology, Nanjing University of Posts and Telecommunications and also a Changjiang Professor with the Department of Control Science and Engineering, Huazhong University of Science and Technology. He is currently an Associate Editor of the IEEE Control Systems Society Conference Editorial Board and also an Associate Editor of the IEEE Transactions on Neural Networks and Learning Systems, the Journal of the Franklin Institute and the International Journal of Systems Science. Up to now, he has published more than 100 papers in international journals, domestic journals, and international conferences. His research interests include analysis and synthesis of networked control systems, multi-agent systems, optimal control of power systems, and internet of things.

Josep M. Guerrero (S'01-M'04-SM'08-FM'15) received the B.S. degree in telecommunications engineering, the M.S. degree in electronics engineering, and the Ph.D. degree in power electronics from the Technical University of Catalonia, Barcelona, in 1997, 2000 and 2003, respectively. Since 2011, he has been a Full Professor with the Department of Energy Technology, Aalborg University, Denmark, where he is responsible for the Microgrid Research Program. From 2012 he is a guest Professor at the Chinese Academy of Science and the Nanjing University of Aeronautics and Astronautics; from 2014 he is chair Professor in Shandong University; and from 2015 he is a distinguished guest Professor in Hunan University.

His research interests is oriented to different microgrid aspects, including power electronics, distributed energy-storage systems, hierarchical and cooperative control, energy management systems, and optimization of microgrids and islanded minigrids; recently specially focused on maritime microgrids for electrical ships, vessels, ferries and seaports. Prof. Guerrero is an Associate Editor for the IEEE TRANSACTIONS ON POWER ELECTRONICS, the IEEE TRANSACTIONS ON INDUSTRIAL ELECTRONICS, and the IEEE Industrial Electronics Magazine, and an Editor for the IEEE TRANSACTIONS on SMART GRID and IEEE TRANSACTIONS on ENERGY CONVERSION. He has been Guest Editor of the IEEE TRANSACTIONS ON POWER ELECTRONICS Special Issues: Power Electronics for Wind Energy Conversion and Power Electronics for Microgrids; the IEEE TRANSACTIONS ON INDUSTRIAL ELECTRONICS Special Sections: Uninterruptible Power Supplies systems, Renewable Energy Systems, Distributed Generation and Microgrids, and Industrial Applications and Implementation Issues of the Kalman Filter; and the IEEE TRANSACTIONS on SMART GRID Special Issue on Smart DC Distribution Systems. He was the chair of the Renewable Energy Systems Technical Committee of the IEEE Industrial Electronics Society. He received the best paper award of the IEEE Transactions on Energy Conversion for the period 2014-2015. In 2014 and 2015 he was awarded by Thomson Reuters as Highly Cited Researcher, and in 2015 he was elevated as IEEE Fellow for his contributions on "distributed power systems and microgrids."